

# Sub-Doppler Stark Spectroscopy in the A–X (1,0) Band of CN<sup>†</sup>

Michael L. Hause, Gregory E. Hall, and Trevor J. Sears\*

Chemistry Department, Brookhaven National Laboratory, Building 555, P.O. Box 5000 Upton, New York 11793-5000

Received: June 29, 2009

The effect of external electric fields has been measured in hyperfine-resolved sub-Doppler transitions in the A <sup>2</sup>Π–X <sup>2</sup>Σ (1,0) band of the CN radical near 10 900 cm<sup>-1</sup>. Static electric fields less than 1 kV/cm are sufficient to mix the most closely spaced Λ-doublets in the A state, leading to Stark spectra with both new and shifted resonances. Simulations of the saturation-dip Stark spectral line profiles allow extraction of the A-state permanent electric dipole moment with a magnitude of 0.06 ± 0.02 D.

## I. Introduction

We have recently used frequency-modulation optical saturation spectroscopy to obtain sub-Doppler spectra of the  $\nu = 1 \leftarrow 0$  band of A <sup>2</sup>Π ← X <sup>2</sup>Σ<sup>+</sup> CN system.<sup>1</sup> Hyperfine splittings observed in a sufficient set of rotational lines, combined with previously measured,<sup>2</sup> X-state hyperfine structure, permitted a determination of a full set of hyperfine and quadrupole parameters for the <sup>14</sup>N nucleus in the CN A state.

The sensitive observation of sharp sub-Doppler resonances offers a means of determining the excited-state electric dipole moment at modest electric fields, well below those required to produce detectable frequency shifts in Doppler-broadened optical transitions. Thomson and Dalby used the Stark splittings induced by the high electric fields inside a discharge source to determine the dipole moments of the X <sup>2</sup>Σ<sup>+</sup> and B <sup>2</sup>Σ<sup>+</sup> states of CN.<sup>3</sup> Since both X and B states are Σ states, with a second-order Stark effect, electric fields up to 130 kV/cm were required to observe Stark splittings for low rotational states in the Doppler-broadened rotational lines. They found the dipole moments of the X and B states to be 1.45(8) and 1.15(8) D, respectively, and they concluded from the relative intensities of several field-induced Q-branch transitions that the X- and B-state dipole moments must have opposite signs. We can use much smaller electric fields, below 1000 V/cm, both because the A <sup>2</sup>Π state has a first-order Stark effect and because the sub-Doppler spectra enable the measurement of much smaller frequency shifts. Previous experimental measurements of the dipole moment of the A state of CN relied upon optical detection of transitions involving A-state levels with  $\nu = 10$  that are perturbed by accidentally nearly degenerate  $\nu = 0$  levels of the B <sup>2</sup>Σ<sup>+</sup> state. Evenson<sup>4</sup> reported  $\mu(\text{A}^2\Pi) < 0.01$  D for  $\nu = 10$  by comparing the relative intensity of electric and magnetic dipole microwave transitions involving perturbed levels, while Cook and Levy<sup>5</sup> reported  $\mu(\text{A}^2\Pi) = 0.56 \pm 0.03$  D for the same quantity, following detailed analysis of some fluorescence-detected level crossings in a magnetic field. Extensive MRCI calculations by Knowles et al.<sup>6</sup> in 1988 found the CN dipole moment in the A state to be considerably smaller in magnitude, and opposite in sign to that of the CN X state. At the equilibrium bond length of the A state they computed  $\mu(\text{A}^2\Pi) = 0.13$  D. More recent calculations by Ajitha and Hirao<sup>7</sup> using a MRCCSD method

approximately agree with this number, although these authors do not actually quote their calculated dipole moment at the equilibrium bond length of the A state. Both calculations report a moderately strong decrease in the dipole moment with increasing bond length.

In this paper, we report Stark shifted sub-Doppler spectra of rotational lines in the A <sup>2</sup>Π–X <sup>2</sup>Σ<sup>+</sup> (1,0) band. By comparing the Stark-broadened spectral contours of the sub-Doppler hyperfine spectra at several electric fields to simulated spectra, we determine the A-state dipole moment. The measurements result in an estimated dipole moment in A <sup>2</sup>Π ( $\nu = 1$ ) of 0.06 ± 0.02 D. This, together with an analysis of the calculated bond length dependence,<sup>6,7</sup> resolves the literature discrepancy in the A-state dipole moment measurements in favor of Evenson's<sup>4</sup> determination for the  $\nu = 10$  level. It is not clear why the dipole moment obtained by Cook and Levy<sup>5</sup> from the analysis of Zeeman anticrossing measurements differs so greatly.

## II. Experiment

Stark spectra of low and intermediate *J*-lines in the (1,0) band of the A <sup>2</sup>Π ← X <sup>2</sup>Σ<sup>+</sup> CN system were collected with sub-Doppler resolution, using a combination of frequency modulation (FM) and saturation spectroscopies.<sup>1,8</sup> A tunable, continuous wave beam near 900 nm (from an argon ion-pumped Coherent MBR 110 Ti:sapphire ring laser) was split into two beams using an uncoated, wedged, fused silica plate. The higher power (100–150 mW) saturation beam passed through an electro-optic amplitude modulator (New Focus, Model 4104) driven sinusoidally at 400 kHz. The lower power (10–15 mW) probe beam passed through an electro-optic phase modulator (New Focus Model 4003) driven at 191.5 MHz. Saturation and probe beams counterpropagated with a crossing angle of 0.5° to allow for independent control of the polarization. The probe beam was collimated to a diameter of 1–2 mm, and the bleach beam was weakly focused to 3–4 mm diameter in the crossing region of the absorption cell. A larger diameter (8 mm) photolysis beam (Lambda-Physics Compex 102, 193.3 nm) overlapped the probe and bleach beams. The photolysis beam dissociated ethanedinitrile (NCCN) (Apogee Technologies, 98.5% purity) to form CN radicals. The flow rates of NCCN into the cell were 0.7–1.0 standard cm<sup>3</sup>/min, resulting in typical pressures of about 50–75 mTorr. With the photolysis power (15–20 mJ) and NCCN pressure, the nascent CN density was about 3 × 10<sup>13</sup> cm<sup>-3</sup>, and the kinetic lifetime in the probed volume was several hundred

<sup>†</sup> Part of the "Robert W. Field Festschrift".

\* Corresponding author. E-mail addresses: G.E.H., gehall@bnl.gov; T.J.S., sears@bnl.gov.

microseconds. The Stark cell contains two stainless steel electrodes 29 cm long and separated by 1.25 cm with Teflon spacers. Voltages applied by direct current (dc) power supply (Bertan Model 313A) were between 250 and 1000 V, giving an electric field between 200 and 800 V/cm. Spontaneous or excimer-laser initiated discharge precluded the use of higher voltages at these NCCN operating pressures and cell geometries.

The detection method used was similar to that described elsewhere.<sup>1</sup> After passing through the sample cell, the probe beam was detected with a fast photodiode (Hamamatsu S3883). A bias-T separated the dc and radio frequency (rf) components of the photocurrent, and an I and Q demodulator produced in-phase (I) and quadrature (Q) components of the 191.5 MHz photodiode signal. The absorption and dispersion signals were isolated in the I and Q channels, respectively, by adjusting the phase of the 191.5 MHz reference local oscillator. For these experiments the dispersion-phase signal was used only for determining the correct phase angle, and the spectral analysis was performed on the absorption phase signals. The 400 kHz amplitude modulation of the bleach laser induces a synchronous variation in the I and Q saturation signals, which were isolated from background with additional amplifiers (LeCroy DA1822A) and mixers (Minicircuit ZAP8+). The mixer output signals were then typically averaged for 40 excimer shots in a LeCroy digital oscilloscope at each dwell frequency of the laser. Voltage steps applied to the piezo drive of the Ti:sapphire internal reference cavity produced laser frequency steps of 1–2 MHz. The control and acquisition program (LabView) also recorded averages of the Ti:sapphire laser wavelength throughout the scan from a wavemeter (Bristol Instruments Series 621A) averaging about 20 measurements per wavelength step.

### III. Results and Analysis

**A. Qualitative Observations.** At the modest electric field strengths (<800 V/cm) of the present study, the X <sup>2</sup>Σ ground state of CN shows negligible Stark splitting, but the near-degeneracy of the parity-doublets in the A <sup>2</sup>Π state can lead to strong mixing at low fields, depending on the magnitude of the A-state dipole moment. The increasing separation of the λ doublet levels at higher J in the A state leads to a reduced Stark effect at higher rotational states; indeed, significant field-dependent changes in the CN (A–X) saturation spectra are only observed for rotational transitions terminating in rotational levels lower than 9/2. Field-dependent spectra terminating in lower rotational states display a growing in of new features on the red for Q branch transitions, and new features on the blue for R and P branch transitions. As the electric field increases, the new features grow in intensity without significant shifting rather than splitting away from existing lines. In addition, the strong and isolated zero-field transitions are observed to broaden as the field increases. To interpret the sub-Doppler Stark spectra and extract an electric dipole moment for the A state, we have modeled the complete hyperfine pattern of selected rotational transitions. We find that the first visible effects at low electric field arise from crossover resonances associated with the parity forbidden transitions, which become allowed as the field mixes nearby levels of opposite parity.

**B. Modeling of Stark Spectra.** The spectra were modeled using an effective Hamiltonian model identical to that described previously<sup>1</sup> but extended to include an operator describing the effects of an external electric field on the molecule. For an external field, E, in the space-fixed z direction, the operator can be written

$$H_{\text{Stark}} = -T_0^1(E) T_0^1(\mu) \quad (1)$$

in the usual notation.<sup>9</sup> As before, we chose to set up the calculation in a parity-conserving case (a) basis set:

$$|\Lambda\Sigma J\Omega IFM_F \pm\rangle = [|\Lambda\Sigma J\Omega IFM_F\rangle \pm (-1)^{J-S} |\Lambda\Sigma -\Sigma J -\Omega IFM_F\rangle] / \sqrt{2} \quad (2)$$

This is the natural basis set for the upper <sup>2</sup>Π state, but not for the lower <sup>2</sup>Σ one, which is almost exactly case (b). Computing transition intensities requires, however, that the two states be described in a common representation, and it is simpler to convert the <sup>2</sup>Σ matrix elements to case (a) than the alternative. Stark Hamiltonian matrix elements in a simple (nonparity conserving) basis set are

$$\langle \Lambda'S'\Sigma'J'\Omega'I'F'M'_F | H_{\text{Stark}} | \Lambda\Sigma J\Omega IFM_F \rangle = -\delta_{M'_F M_F} \delta_{I'I} \delta_{S'S} E_0 \langle \mu \rangle (-1)^{F'-M'_F} \begin{pmatrix} F' & 1 & F \\ -M'_F & 0 & M_F \end{pmatrix} \times (-1)^{J'+I'+F+1} [(2F'+1)(2F+1)]^{1/2} \begin{Bmatrix} I & J' & F' \\ 1 & F & J \end{Bmatrix} (-1)^{J'-\Omega} [(2J'+1)(2J+1)]^{1/2} \begin{pmatrix} J' & 1 & J \\ -\Omega & 0 & \Omega \end{pmatrix} \quad (3)$$

where it has been assumed that the direction of the dipole moment, ⟨μ⟩, is along the internuclear bond, the molecule-fixed z direction. In the parity-conserving basis set we use, the nonzero Stark Hamiltonian matrix elements couple basis vectors of opposite parity belonging to more than one zero-field F level. |M<sub>F</sub>| is now the good quantum number and the Stark matrix is in principle infinite. For the calculation at a given M<sub>F</sub> in the low rotational levels of interest, restricting the coupled basis vectors to those with |ΔF| ≤ 2 allowed convergence of the eigenvalues well within the experimental accuracy.

Stark shifted energy levels for the hyperfine and parity components of the A<sup>2</sup>Π<sub>3/2</sub>, J = 5/2 rotational level are illustrated in Figure 1, as a function of the Stark interaction strength, expressed in (Debye kV)/cm units. We see the zero-field energies of the F = 3/2(–) level and the F = 5/2(+) level are less than 3 MHz apart, while the F = 5/2(–) and F = 7/2(+) levels are separated by about 13 MHz. Avoided crossings between identical M<sub>F</sub> components of these two nearly degenerate pairs of states occur in order as the field is increased. This effect makes spectroscopic transitions terminating in J = 5/2 particularly sensitive to Stark effects at small electric fields. In the A<sup>2</sup>Π<sub>3/2</sub>, J = 5/2 level, the Stark-induced mixing between the F = 3/2(–) and the F = 5/2(+) levels results

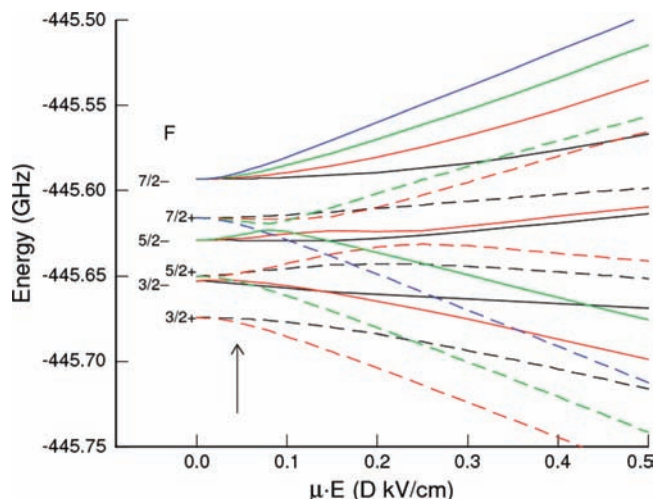


**Figure 1.** Calculated Stark splitting of the hyperfine and parity components of CN ( $A^2\Pi_{3/2}$ ,  $v = 1$ ,  $J = 5/2$ ). The zero-field hyperfine levels are labeled by  $F$  and parity, dashed and solid lines depict correlation to zero-field levels of  $+$  and  $-$  parities, and the colors (online) label states of the same  $M$ . The vertical arrow labels a region near the observed pattern at a laboratory field of 800 V/cm. The energy is relative to an origin midway between the rotationless  $^2\Pi_{3/2}$  and  $^2\Pi_{1/2}$  fine structure levels, approximately  $A/2$ , where  $A$  is the spin-orbit constant (a negative quantity for A-state CN).<sup>10</sup>

in the zero-field electric-dipole forbidden parity transitions gaining intensity even at very small electric fields as parity is no longer a good quantum number. The spectral features associated with full mixing of the  $F = 5/2(-)$  and  $F = 7/2(+)$  are not observed at our maximum field of 800 V/cm, providing secure bounds on the A-state dipole moment. We note that a dipole moment as large as 0.56 D, as reported by Cook and Levy<sup>5</sup> would produce massively larger Stark splittings than we observe at our electric field conditions, sampling energies at the right-hand margin of Figure 1.

The situation is illustrated in Figures 2 and 3 for the  $Q_1(5/2)$  transitions. In zero field (Figure 2) transitions between the hyperfine levels of  $X^2\Sigma^+$ ,  $J = 5/2(+)$ , which is the  $F_1$  fine structure component of  $N = 2$  in a (more natural) case (b) representation, only terminate in  $(-)$  parity levels as shown. In our experiment, we also see crossover resonances that result from transitions sharing a common upper or lower hyperfine component.<sup>1</sup> A common lower-state crossover resonance, for example, arises when a depleted velocity group produced by the bleach laser on one transition matches the sideband-probed velocity group of the common lower level, as probed on a transition to a different upper state. The crossover resonances occur midway between the simple two-level saturation resonances, with an intensity given by the geometric mean of the two simple resonances. We have modeled the intensities of the various hyperfine components by setting up the matrix of the transition dipole moment operator between the connected hyperfine levels in the same basis set as used for the energy level calculations, then applying the transformation matrix resulting from the eigenvalue calculation. Crossover transition intensities were computed as the geometric mean of the intensity calculated for the individual pair of transitions they are derived from, while their frequency is just the average of the two individual ones. Finally, the individual transitions were convolved using a Lorentzian line shape function:

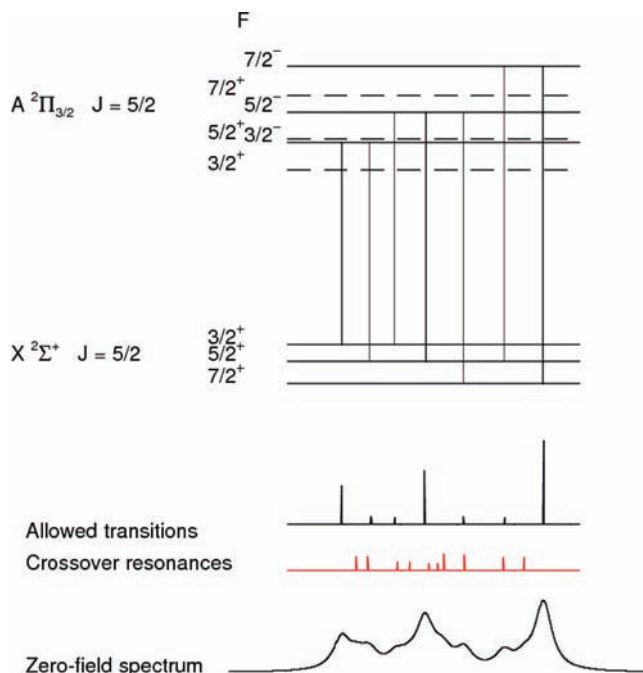


**Figure 2.** Hyperfine and parity sublevels probed in the  $Q_1(5/2)$  transition. The lower energy ( $+$ ) parity levels depicted with dashed lines are not observed in the zero-field Q-branch spectrum. Thick and thin vertical lines depict strongly allowed  $\Delta F = \Delta J$  and weakly allowed  $\Delta F = \Delta J \pm 1$  transitions. Stick spectra below indicate the strong and weak allowed transitions, and the crossover resonances. The synthetic spectrum below is obtained by convolving the total stick spectrum with a 4.5 MHz Lorentzian line width.

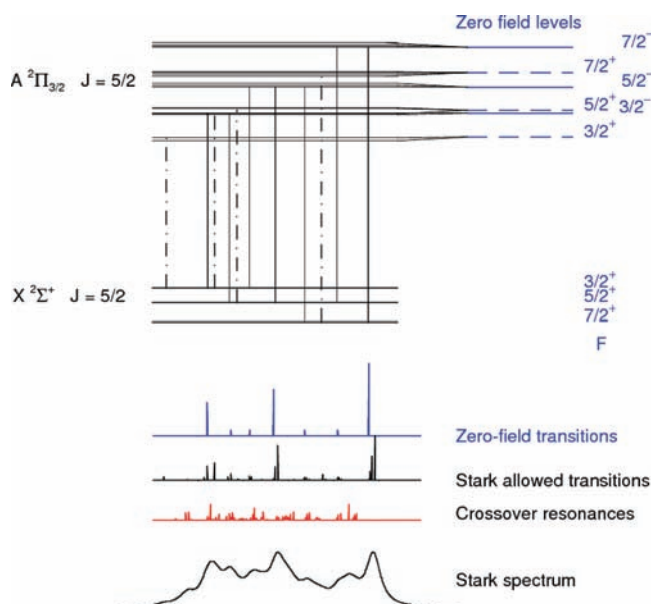


**Figure 3.** Calculated Stark spectrum for the  $Q_1(5/2)$  transition. The Stark levels of the A state are for  $\mu E = 50$  D V cm<sup>-1</sup>, comparable to the pattern observed at 800 V/cm. Dot-dashed vertical lines indicate the field-induced lines derived from parity-forbidden transitions. The zero field stick spectrum is repeated from Figure 2 for reference with the Stark spectra below.

$$L(\nu) = \left(\frac{1}{\pi}\right) \left( \frac{\alpha_L}{(\nu - \nu_0)^2 + \alpha_L^2} \right) \quad (4)$$

where  $\alpha_L$  is the Lorentzian half-width, taken to be 4.5 MHz in the current experiments and  $\nu_0$  is the transition rest frequency. Under our experimental conditions of pressure, beam crossing



geometry, and bleach laser intensity, the intensity of the saturation lines remains an approximately linear function of the bleach laser intensity, and the calculated transition intensities of weak and strong hyperfine transitions. At lower pressures or higher saturation laser intensities, the sub-Doppler spectra become nonlinear in the saturation laser intensity, and a more sophisticated intensity model would be required.

Figure 2 illustrates the way in which the spectrum simulation is built up for the zero field spectra, while Figure 3 shows the same transition when an electric field is applied. In Figure 3, we see that the crossover transitions between the strongly allowed  $\Delta J = \Delta F$  hyperfine components and the weak, field-induced, parity-forbidden transitions resulting from electric field mixing of different parity levels in the excited state are the first observable manifestation of the Stark effect in this transition.

In these spectral simulations, the only unknown quantity is the dipole moment of the excited state. It always appears as a product with the electric field,  $E$ , so that simulations for a series of values of this product may be compared against the observed Stark spectra and an estimate of the dipole moment made. Figure 4 makes this comparison for the  $Q_1(5/2)$  transition explicitly, for the spectrum observed in zero field, and at a field of 800 V/cm for a series of assumed values of the dipole moment. A best-fit value of 0.06 D is illustrated along with larger and smaller trial values leading to contours that differ enough to reject as consistent with our observations, particularly based on the spectral features between 140 and 200 MHz relative frequency offset in the figure. Since individual scans were recorded at a series of fixed electric fields, our measurements are better at comparing peak shapes and splittings within individual spectra than the precise field-dependent shifts, which occur at the level of a few megahertz. Lower electric field measurements of the same transition are consistent but have fewer distinctive features.

We have measured Stark spectra for a number of additional transitions, including  $R_1(3/2)$ ,  $P_1(7/2)$  and  $Q_1(7/2)$ . The analyses are consistent with that for  $Q_1(5/2)$ , but less quantitative, since simulations of these spectra show less distinctive changes in the band contours with electric field than for the Q line. The predicted new crossover resonances at frequencies higher than those of the zero field spectrum, due to field-induced, parity-forbidden transitions, are experimentally confirmed, but fewer spectra were recorded and signal-to-noise ratios were less favorable for the P and R-branch transitions.

#### IV. Discussion

Our modeling of the observed Stark spectra of the  $Q_1(5/2)$  line at fields up to 1000 V/cm results in an estimated dipole moment of  $0.06 \pm 0.02$  D. The error in this determination is difficult to quantify precisely, since the comparison of simulation and experiment involves band contour matching rather than a pure frequency domain measurement. Our best limits come from the  $Q_1(5/2)$  contour analysis. The predicted patterns in the spectrum at higher field (or larger trial dipole moment) would be distinctive when the  $F = 5/2(-)$  and the  $F = 7/2(+)$  levels mix most strongly at around 0.1 D kV/cm, placing a secure upper bound near 0.08 D. A dipole moment less than 0.04 would be insufficient to account for the strength of the parity forbidden transitions. The accuracy of the model depends on a precise knowledge of the zero-field parity and hyperfine splittings. These come from the work of Cerny et al.<sup>10</sup> and our previous measurements<sup>1</sup> of the hyperfine splittings. In terms of the calculated Stark shifts, the parity spacings in the upper state level, shown in Figures 1–3, are of most concern. We computed

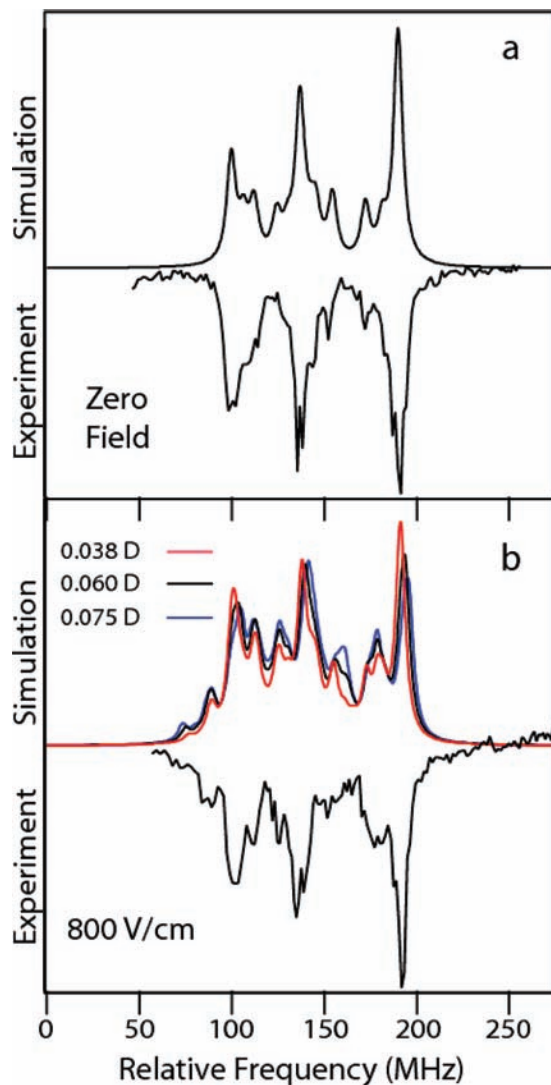


**Figure 4.** Observed and calculated hyperfine spectra of the  $Q_1(5/2)$  line: (a) zero-field spectrum; (b) experimental 800 V/cm spectrum and simulation for three trial A-state dipole moments. An assumed dipole moment of 0.06 D produces a superior match to the experiment than the larger or smaller values illustrated.

energy levels using  $\Lambda$ -doubling parameters differing by the two standard deviations quoted by Cerny et al.<sup>10</sup> and found zero field energy differences were of the order of 100 kHz, i.e., negligible on the scale of our measurement precision. The observed frequencies of the field-induced crossover resonances are our most direct test of the zero-field parity splittings, and we find agreement within our measurement errors of 1–2 MHz. For the ground state, the Stark level shifts and splittings are very small at the fields used in this work; they were computed as described above but play no role in the observed spectral changes as the field is applied. Hence we are confident of the numerical reliability of our Stark spectral simulations.

Previous experimental determinations of the A-state dipole moment by Evenson<sup>4</sup> and Cook and Levy,<sup>5</sup> both of which involved the  $\nu = 10$  excited level, differ by a factor of more than 50. Our experimental estimate is an order of magnitude smaller than Cook and Levy, but still larger than Evenson's upper limit by a factor of at least 5. We may reconcile the current measurement with Evenson's by examining the variation of the computed<sup>6,7</sup> A-state dipole moment with bond length. Table 2 of Knowles et al.<sup>6</sup> gives the A-state dipole moment computed as a function of the bond length. From the results of Prasad

and Bernath,<sup>11</sup> we can estimate the effective bond lengths at equilibrium and for various vibrational levels. We find  $r_0 = 1.236$ ,  $r_1 = 1.242$ , and  $r_{10} = 1.305$  Å, where the subscripts refer to the vibrational level in the A state. Interpolating from the results of reference,<sup>6</sup> we estimate  $\mu_0 = 0.13$  D,  $\mu_1 = 0.12$  D, and  $\mu_{10} = 0.005$  D, close to our  $\nu = 1$  measurement, although somewhat larger than can be reconciled with our estimated error, and also Evenson's result<sup>4</sup> for the perturbed  $\nu = 10$  level. Similar numbers can be derived from the more recent MRCCSD calculation of Ajitha and Hirao.<sup>7</sup> Here, a short extrapolation from results for the bond lengths they consider (generally more appropriate for the ground state of the radical) gives  $\mu_1 = 0.08$  D and  $\mu_{10} = -0.04$  D, the negative sign indicating that the direction of the dipole has changed. In summary, the present result is largely consistent with both the published computational studies and the earlier experimental estimate. The Cook and Levy result is inconsistent. It derives from the measurement of magnetic field-induced changes in fluorescence from perturbed levels of  $B^2\Sigma^+$  CN in the presence of an electric field and required extensive modeling to extract the dipole moment. We postulate that the observed spectrum may not be due to the assigned avoided crossings. A further reason for suspicion in their interpretation is a discrepancy in radiative lifetimes. As acknowledged by Cook and Levy, the A-state lifetime inferred from related anticrossing experiments<sup>12</sup> differs significantly from other more direct measurements. Knowles et al.<sup>6</sup> calculated the vibrational dependence of A- and B-state fluorescence lifetimes, in agreement with most direct lifetime measurements, but not the values derived from Cook and Levy's analysis.

In the present measurements, we have depended on modeling the appearance of new Stark-induced features and broadening in the observed spectra rather than traditional spectroscopic methods that measure line frequency shifts. The absolute frequencies of the main features of the spectrum do indeed shift at the fields used in the present work; however, we are not able to measure the absolute frequency of the optical transition with sufficient precision to take advantage of this. An alternative scheme in which a field on–field off spectrum could be collected in a time short compared to drift in the absolute laser position over periods of several minutes would permit reliable measurement of the small frequency shifts, as would referencing the laser to a stable frequency source such as a frequency comb.<sup>13</sup>

The present method could be adopted for any radical with an orbitally degenerate electronic state where the Stark effect is approximately first order. CN in its  $A^2\Pi$  state has a small dipole moment; sub-Doppler measurements on a similar species with a larger dipole moment would show considerably larger effects, even at the low fields employed here. Dipole moment measurements for excited-state radicals are quite rare. Steimle has performed extensive high resolution Stark LIF studies on supersonically cooled and collimated beams of metal containing

radicals, typically with very large dipole moments.<sup>14</sup> Gray et al.<sup>15</sup> reported a measurement of the dipole moment of  $A^2\Sigma^+$  NO using a Stark fluorescence quantum beat experiment, but this required large electric fields because the Stark effect in even the lowest  $^2\Sigma$  levels is small, as it is in the  $^2\Sigma$  ground state of CN.

## V. Conclusions

We have determined the dipole moment for the A state of CN by modeling the observed Stark-broadened contours of sub-Doppler hyperfine-resolved spectra at several electric fields. The measurements and their analysis result in an estimated dipole moment in  $A^2\Pi$  ( $\nu = 1$ ) of  $0.06 \pm 0.02$  D. This, together with an analysis of the calculated bond length dependence,<sup>6,7</sup> resolves the literature discrepancy in the A-state dipole moment measurements in favor of Evenson's<sup>4</sup> determination for the  $\nu = 10$  level. It is not clear why the dipole moment obtained by Cook and Levy<sup>5</sup> from the analysis of Zeeman anticrossing measurements differs so greatly. Our result agrees within the error limits to the value recently computed<sup>7</sup> but is slightly, but significantly, smaller than the MRCI results of Knowles et al.<sup>6</sup> Their computed bond length dependence of the dipole moment qualitatively reproduces the observed change in dipole moment in  $\nu = 1$  determined here, to  $\nu = 10$  of Evenson's work.

**Acknowledgment.** This work was carried out at Brookhaven National Laboratory under Contract No. DE-AC02-98CH10886 with the U.S. Department of Energy, Office of Science, and supported by its Division of Chemical Sciences, Geosciences, & Biosciences within the Office of Basic Energy Sciences.

## References and Notes

- (1) Hause, M. L.; Hall, G. E.; Sears, T. J. *J. Mol. Spectrosc.* **2009**, *253*, 122.
- (2) Dixon, T. A.; Woods, R. C. *J. Chem. Phys.* **1977**, *67* (9), 3956.
- (3) Thomson, R.; Dalby, F. W. *Can. J. Phys.* **1968**, *46*, 2815.
- (4) Evenson, K. M. *Phys. Rev.* **1969**, *178*, 1.
- (5) Cook, T. J.; Levy, D. H. *J. Chem. Phys.* **1973**, *59*, 2387.
- (6) Knowles, P. J.; Werner, H.-J.; Hay, P. J.; Cartwright, D. C. *J. Chem. Phys.* **1988**, *89*, 7334.
- (7) Ajitha, D.; Hirao, K. *Chem. Phys. Lett.* **2001**, *347*, 121.
- (8) Hall, J. L.; Holberg, L.; Baer, T.; Robinson, H. G. *Appl. Phys. Lett.* **1981**, *39*, 680.
- (9) Brown, J. M.; Carrington, A. *Rotational Spectroscopy of Diatomic Molecules*; Cambridge University Press: Cambridge, U.K., 2003.
- (10) Cerny, D.; Bacis, R.; Guelachvili, G.; Roux, F. *J. Mol. Spectrosc.* **1978**, *73*, 154.
- (11) Prasad, C. V. V.; Bernath, P. F. *J. Mol. Spectrosc.* **1992**, *156*, 327.
- (12) Cook, T. J.; Levy, D. H. *J. Chem. Phys.* **1972**, *57* (12), 5059.
- (13) Cundiff, S. T.; Ye, J. *Rev. Mod. Phys.* **2003**, *75*, 325.
- (14) Steimle, T. C. *Int. Rev. Phys. Chem.* **2000**, *19* (3), 455.
- (15) Gray, J. A.; Farrow, R. L.; Durant, J. L.; Thorne, L. R. *J. Chem. Phys.* **1993**, *99*, 4327.

JP906085E